



Fermi National Accelerator Laboratory

FERMILAB-Conf-92/146-E

QCD Physics at CDF

**The CDF Collaboration
Presented by R. Harris**

*Fermi National Accelerator Laboratory
P.O. Box 500, Batavia, Illinois 60510*

May 1992

To appear in the proceedings of the XXVII Rencontre de Moriond, Les Arcs, France, 1992.

Disclaimer

This report was prepared as an account of work sponsored by an agency of the United States Government. Neither the United States Government nor any agency thereof, nor any of their employees, makes any warranty, express or implied, or assumes any legal liability or responsibility for the accuracy, completeness, or usefulness of any information, apparatus, product, or process disclosed, or represents that its use would not infringe privately owned rights. Reference herein to any specific commercial product, process, or service by trade name, trademark, manufacturer, or otherwise, does not necessarily constitute or imply its endorsement, recommendation, or favoring by the United States Government or any agency thereof. The views and opinions of authors expressed herein do not necessarily state or reflect those of the United States Government or any agency thereof.

QCD Physics at CDF The CDF Collaboration*

Presented by Robert M. Harris[†]
*Fermi National Accelerator Laboratory
Batavia, Illinois 60510*



ABSTRACT

We present measurements of jet production and isolated prompt photon production in $\bar{p}p$ collisions at $\sqrt{s} = 1.8$ TeV from the 1988-89 run of the Collider Detector at Fermilab (CDF). To test QCD with jets, the inclusive jet cross section ($\bar{p}p \rightarrow J + X$) and two jet angular distributions ($\bar{p}p \rightarrow JJ + X$) are compared to QCD predictions and are used to search for composite quarks. The ratio of the scaled jet cross sections at two Tevatron collision energies ($\sqrt{s} = 546$ and 1800 GeV) is compared to QCD predictions for X_T scaling violations. Also, we present the first evidence for QCD interference effects (color coherence) in third jet production ($\bar{p}p \rightarrow JJJ + X$). To test QCD with photons, we present measurements of the transverse momentum spectrum of single isolated prompt photon production ($\bar{p}p \rightarrow \gamma + X$), double isolated prompt photon production ($\bar{p}p \rightarrow \gamma\gamma + X$), and the angular distribution of photon-jet events ($\bar{p}p \rightarrow \gamma J + X$). We have also measured the *isolated* production ratio of η and π^0 mesons ($\bar{p}p \rightarrow \eta + X$)/($\bar{p}p \rightarrow \pi^0 + X$) = $1.02 \pm .15(stat) \pm .23(sys)$.

* The CDF collaboration: ANL - Brandeis - University of Chicago - Fermilab - INFN, Frascati - Harvard - University of Illinois - KEK - LBL - University of Pennsylvania - INFN, University of Scuola Normale Superiore of Pisa - Purdue - Rockefeller - Rutgers - Texas A&M - Tskuba - Tufts - University of Wisconsin
[†] Supported by the U.S. Department of Energy, contract number DE-AC02-76CH03000.

1. Testing QCD with Jets

1.1. Inclusive Jet Cross Section

The CDF ¹⁾ measurement of the inclusive jet cross section is primarily used as a test of QCD and a constraint on parton distribution functions (PDFs). The next-to-leading-order (NLO) calculations ^{2) 3) 4)} of jet production are much less sensitive to the choice of renormalization scale than the leading order calculation, allowing us to make a tighter constraint on PDFs. Also, the jet P_T distribution has been used to search for quark substructure, a signal of new physics beyond the standard model. If quarks are composite particles then, according to conventional theory, ⁵⁾ a contact term of unit strength between left-handed quarks is added to the Lagrangian for interactions at energies less than the compositeness energy scale Λ_C . This contact term, which is independent of P_T in contrast to the QCD interaction term which decreases as $1/P_T^4$, would produce an excess rate at high P_T : the signal for quark substructure.

Jets are defined as the energy inside a cone of radius $R = \sqrt{(\Delta\eta)^2 + (\Delta\phi)^2} = 0.7$ centered on the jet transverse energy centroid. The NLO QCD calculation uses a similar definition, in which two partons are merged if they fall inside the cone. We measure $E_T = E \sin\theta$, and correct the E_T spectrum for calorimeter response (non-linearities and cracks), underlying event energy inside the jet cone, and energy resolution smearing of the spectrum. The uncertainties in E_T and in $d\sigma/dE_T$ are shown in Fig. 1; note that the uncertainty in $d\sigma/dE_T$ is predominantly systematic at low E_T and statistical at high E_T . The CDF measurement of the inclusive jet cross section ⁶⁾ is shown in Fig. 2a, in comparison to a NLO QCD prediction ²⁾ and LO QCD plus composite quarks. The data agrees with NLO QCD over 7 orders of magnitude and we do not see a statistically significant signal for quark substructure. We set the limit $\Lambda_C > 1.4$ TeV at 95% confidence level (twice our previously published ⁷⁾ limit). In Fig. 2b we compare our measurement to NLO QCD calculations with three recent PDFs. ⁸⁾ The data is in good agreement with all PDFs except HMRS set E.

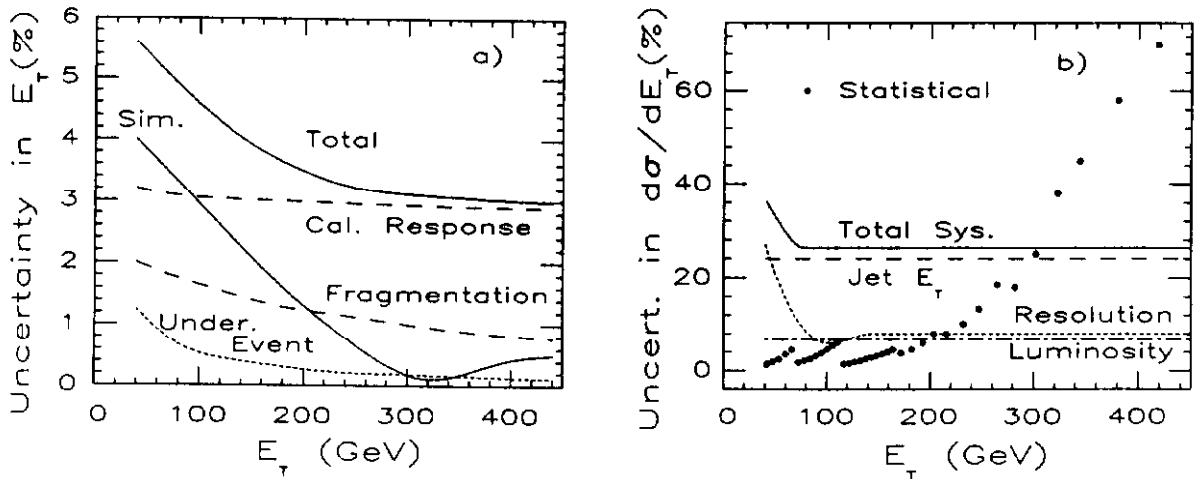


Figure 1: a) The upper systematic uncertainties on jet E_T . b) The uncertainties, systematic and statistical, in the jet cross section vs. E_T .

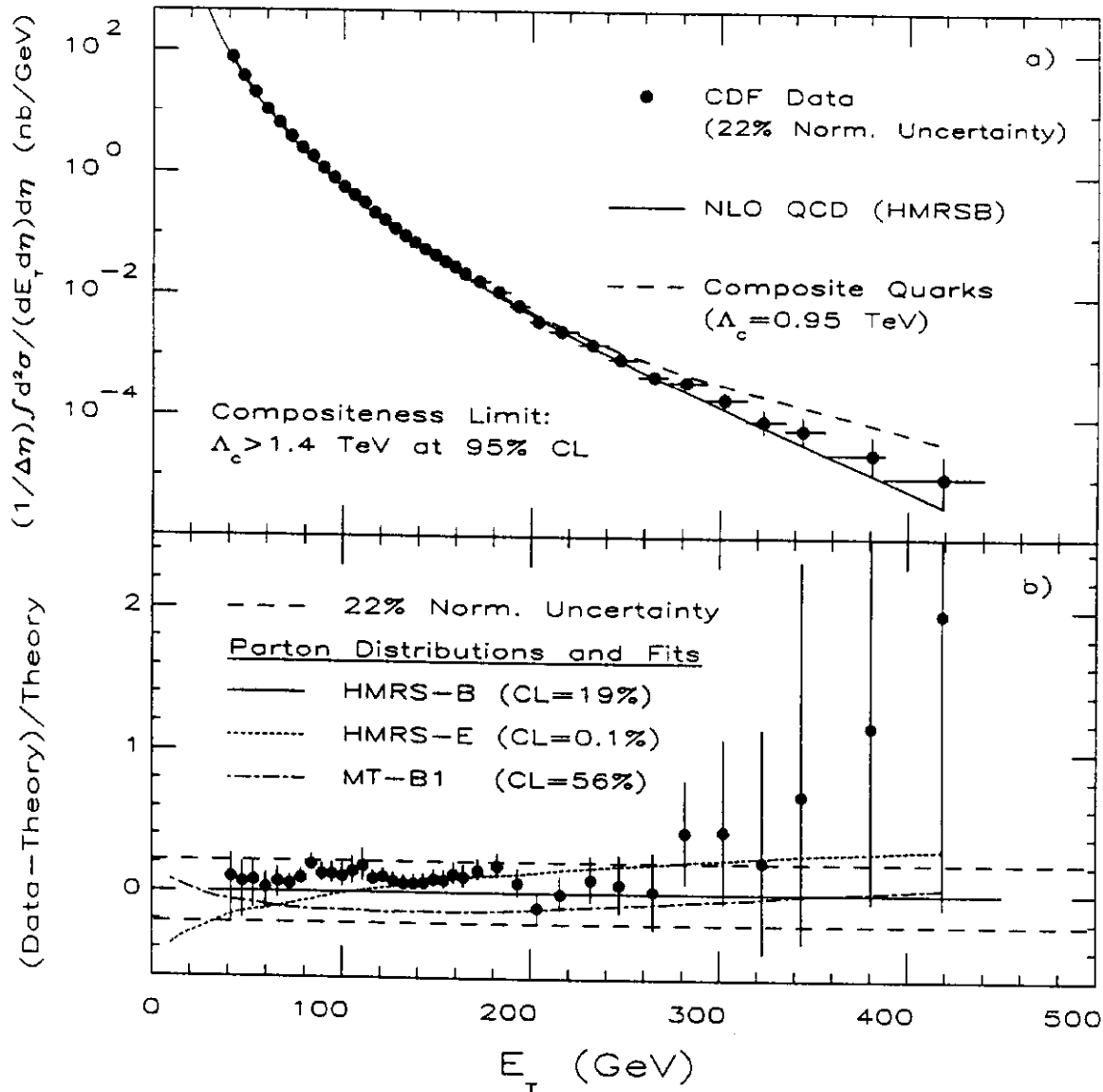


Figure 2: The inclusive jet cross section vs. E_T compared with a) NLO QCD and LO QCD plus compositeness and b) NLO QCD with a variety of parton distribution functions.

1.2. Two Jet Angular Distributions

Additional information about QCD and limits on quark compositeness can be obtained from two jet angular distributions. We employ the three orthogonal CMS variables:

$$\eta^* = (\eta_1 - \eta_2)/2, \quad \eta_{boost} = (\eta_1 + \eta_2)/2, \quad M_{jj} = \sqrt{(E_1 + E_2)^2 + (\bar{P}_1 + \bar{P}_2)^2} \quad (1)$$

Where E_i , \bar{P}_i and η_i are the energy, momentum and pseudorapidity of jet i (E_T ordered). The angular variable $\chi = \exp 2|\eta^*|$ is particularly useful because $dN/d\chi$ is perfectly flat for Rutherford scattering and hence roughly flat for QCD scattering of partons. The signal for composite quarks is a $dN/d\chi$ distribution which peaks sharply at low χ .

The analysis seeks to maximize the range in χ , while maintaining full acceptance and avoiding the crack between the forward and plug calorimeters. This results in the cuts $|\eta^*| < 1.6$ and $|\eta_{boost}| < 0.75$ which corresponds to a maximum jet pseudorapidity of 2.35. In Fig. 3 we plot the jet angular distribution for three intervals of two jet mass

M_{jj} ; the trigger was fully efficient for these mass intervals. The distributions have been corrected for the acceptance in χ , which is flat to within roughly 5%, with a systematic uncertainty of less than 10% (dominated by the uncertainty in the jet energy as a function of pseudorapidity). The angular distributions in Fig. 3 are compared to QCD predictions ²⁾ at leading order (LO), NLO, and LO plus composite quarks. The confidence levels for QCD are quite reasonable, and we set the compositeness limit $\Lambda_C > 1.0$ TeV at 95% confidence level (three times our previously published limit ⁹⁾ from this channel).

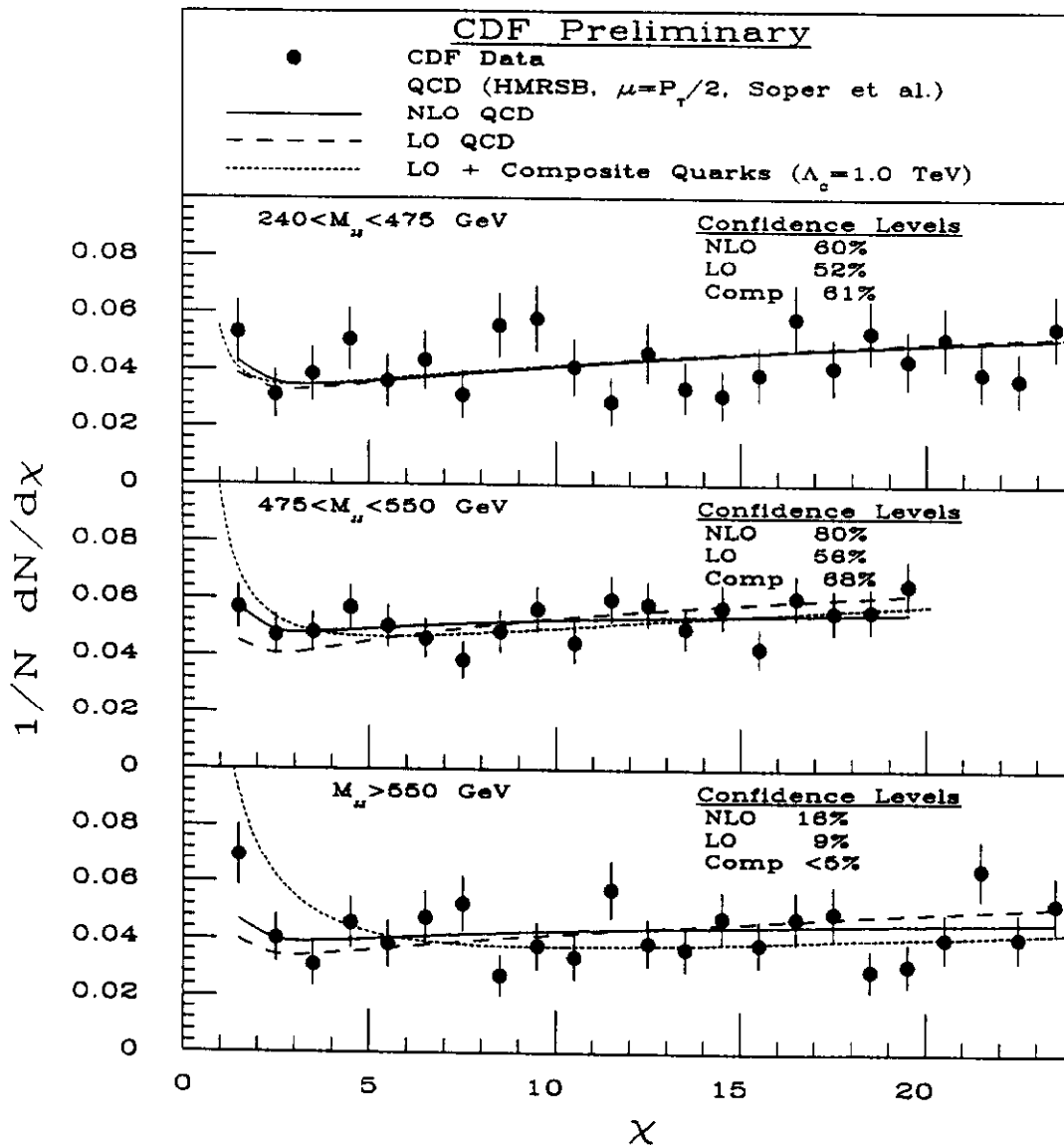


Figure 3: The two jet angular distribution, for three mass intervals, compared to the predictions of QCD and QCD plus composite quarks, and the resulting confidence levels.

1.3. X_T Scaling Violations

The naive parton model, without QCD evolution, predicts that the scaled jet cross section, $\sigma' = P_T^4 (Ed^3\sigma/dp^3)$ plotted vs. $X_T = 2P_T/\sqrt{s}$ will be the same at every value of \sqrt{s} . Thus, X_T scaling naively predicts that the ratio of scaled cross sections $\sigma'(\sqrt{s} = 546 \text{ GeV})/\sigma'(\sqrt{s} = 1800 \text{ GeV})$ is 1. CDF has accumulated 8.6 nb^{-1} of data at $\sqrt{s} = 546 \text{ GeV}$

to test scaling, and more important, to test the QCD prediction of X_T scaling violations. At a fixed X_T the renormalization scale, $\mu \approx P_T = X_T\sqrt{s}/2$, depends on \sqrt{s} , hence scaling violations are predicted by both the running of the strong coupling ($\alpha_s(\mu)$) and the evolution of the PDFs. The two effects contribute roughly equally in our range of X_T , and combine to predict a ratio of roughly 1.8 instead of the value 1 predicted by scaling.

The analysis of the $\sqrt{s} = 546$ GeV data proceeds analogously to the analysis of the $\sqrt{s} = 1800$ GeV data. All the corrections are the same, with the exception that the jet response function at 546 GeV is slightly different to account for the softer underlying event. The systematic uncertainties on the $\sqrt{s} = 1800$ GeV data have been re-evaluated in light of an improved understanding of calorimeter response resulting from additional testbeam analysis. In Fig. 4 we show the systematic uncertainties on the cross section at $\sqrt{s} = 546$ GeV, 1800 GeV, and on the ratio of scaled cross sections. Note the dramatic reduction in systematic uncertainties when measuring the ratio.

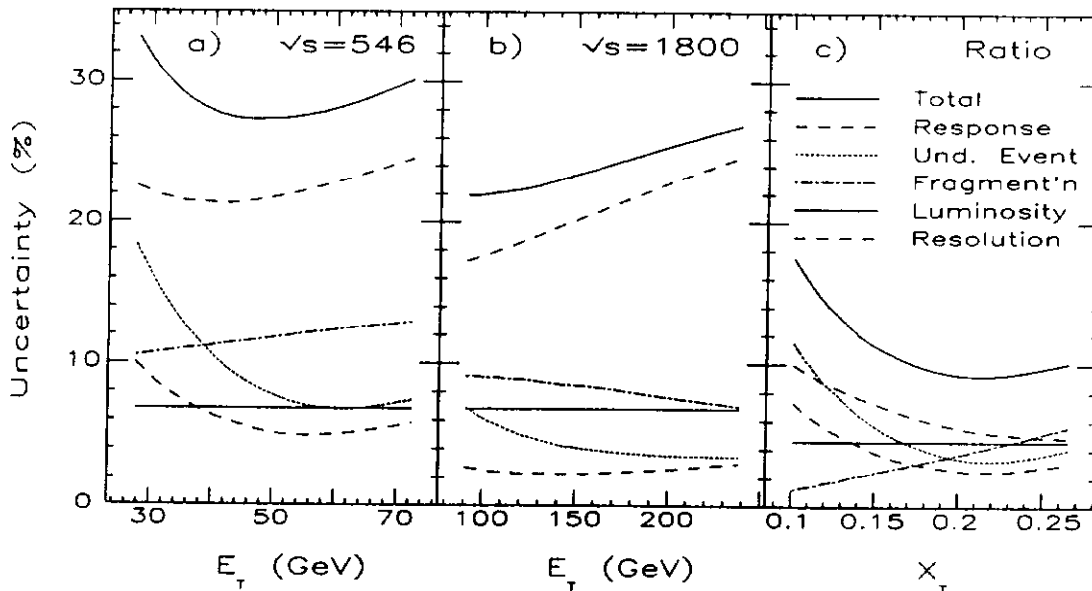


Figure 4: The systematic uncertainty in the CDF measurement of the inclusive jet cross section at a) $\sqrt{s} = 546$ GeV and b) 1800 GeV and c) the ratio of the scaled cross sections.

In Fig. 5a we present the inclusive cross section at $\sqrt{s} = 546$ GeV from CDF compared to that from UA2¹⁰⁾ (same \sqrt{s}). Normalization uncertainties are shown in the legend. The CDF data are shown with two definitions of corrected jet E_T , the first is the conventional CDF definition in which the measured jet E_T is corrected to equal the E_T of the particles inside the jet cone, and the second is the UA2 definition of jet P_T in which the measured jet E_T is corrected to equal the P_T of the “original massless parton” as defined by ISAJET. When CDF uses the UA2 definition of jet E_T the two results agree. However, in order to carry out a consistent comparison with NLO QCD it is necessary to use the CDF definition, which does not add in energy falling outside the jet cone (the theory does not add in radiation falling outside the cone).

In Fig. 5b we present our measurement of the ratio of scaled jet cross sections at $\sqrt{s} = 546$ and 1800 GeV. The error bars are statistical and the hatched band is the systematic uncertainty. The data is compared to next-to-leading order QCD calculations,²⁾ using one set of recent PDFs and shown for three different values of the renormalization scale μ , and is also compared to the scaling hypothesis. Clearly, the data is not in

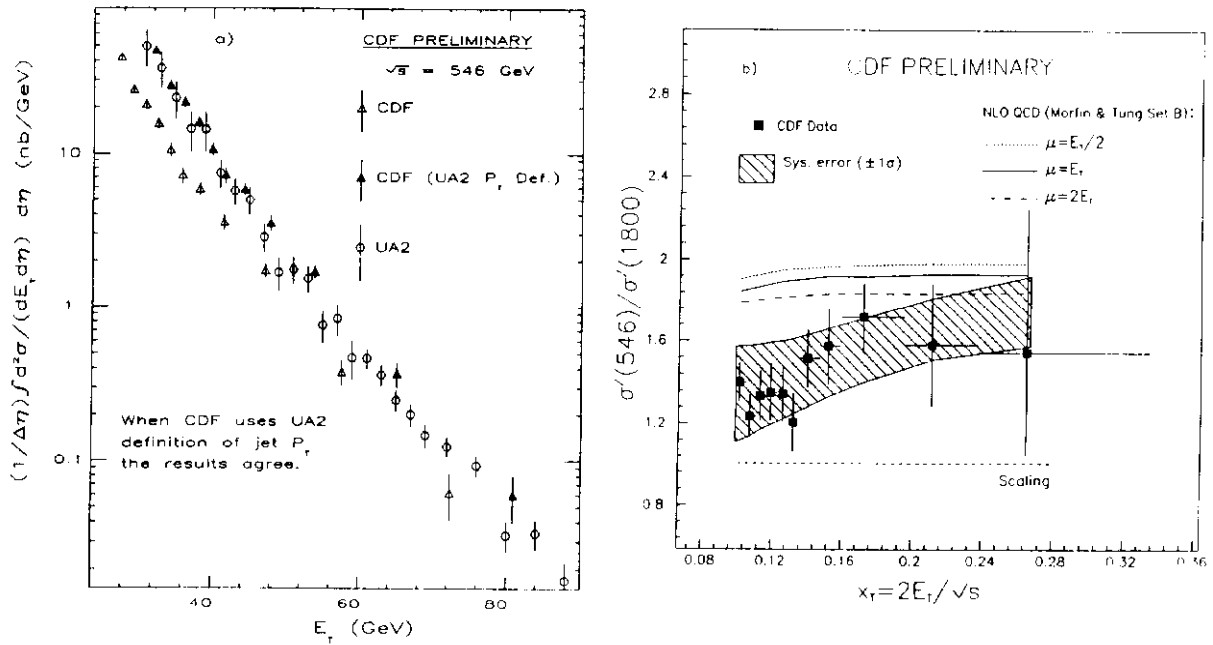


Figure 5: a) The inclusive jet cross section at $\sqrt{s} = 546$ GeV from CDF and UA2 (see text). b) The ratio of scaled jet cross section from CDF at $\sqrt{s} = 546$ GeV and 1800 GeV compared to the predictions of scaling and NLO QCD.

good agreement with either the scaling hypothesis or the QCD prediction for scaling violations. This result is preliminary, and the statistical and systematic significance of the discrepancy between data and QCD is still being evaluated.

1.4. Interference Effects in QCD Radiation (Color Coherence)

We use events with three jets to study interference between processes with soft gluon radiation in the initial and final state shown in Fig. 6a. In theory, interference can always occur when the initial and final state are *color connected*¹¹⁾ (a color line can be traced from the initial to final state). In Fig. 6b we illustrate how radiation tends to occur within cones centered on color lines, and where the cones overlap there is an enhancement of radiation (constructive interference).¹²⁾ Hence, we search for an enhancement of third jet production in the radiation enhanced region between the second jet and the $\bar{p}p$ beam, shown in Fig. 6c.

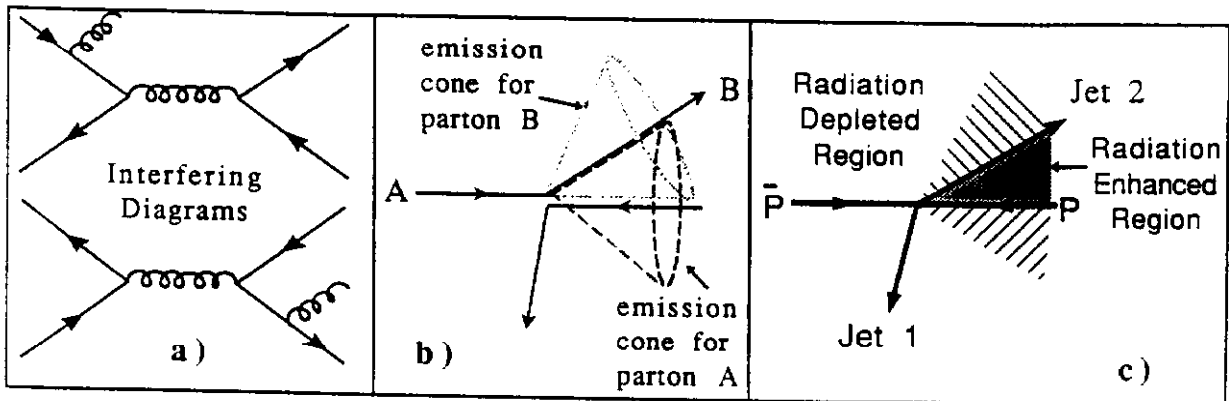


Figure 6: a) Some interfering diagrams that produce a soft third jet. b) Radiation emission cones for initial state parton A and final state parton B. c) Overlapping cones produce a region of enhanced third jet production.

We order jets in E_T , and require jet 1 to have $E_T > 110$ GeV for an efficient trigger. Jets 1 and 2 are required to be central ($|\eta| < 0.7$) and opposite in ϕ to within 20° (this cut suppresses hard radiation). Jet 3 is required to have $E_T > 10$ GeV, leaving us with a sample of three jet events consisting of energetic leading jets (1 and 2) and a soft third jet, probably from soft gluon radiation. The separation between the 2nd and 3rd jet in pseudorapidity is $H = \text{sign}(\eta_2)(\eta_3 - \eta_2)$, and in azimuth is $\Phi = \phi_3 - \phi_2$. The signal for interference is best displayed in terms of the polar variables $R = (H^2 + \Phi^2)^{1/2}$ and $\alpha = \arctan(H/|\Phi|)$. We require $1.1 < R < \pi$ to obtain reasonably uniform acceptance vs. α .

In Fig.7 we plot the variable α in comparison to Montecarlo predictions with and without QCD interference effects. From phase space considerations alone we would expect the α distribution to have a negative slope, as illustrated by the ISAJET¹³⁾ montecarlo (dashed curve) which does not include QCD interference effects. The montecarlo HERWIG¹⁴⁾ (solid curve) includes QCD interference effects, and shows an increase towards positive slope of the α distribution as α increases towards $\pi/2$, in rough agreement with CDF data. As a check that this difference between ISAJET and HERWIG is due primarily to QCD interference effects, we remove events from HERWIG that produce interference (events with particles that are color connected to both the initial and final state partons), and the remaining events (dotted curve) look like ISAJET. We conclude that the data shows an effect compatible with QCD interference. This is the first observation of a color coherence effect at $\bar{p}p$ colliders.

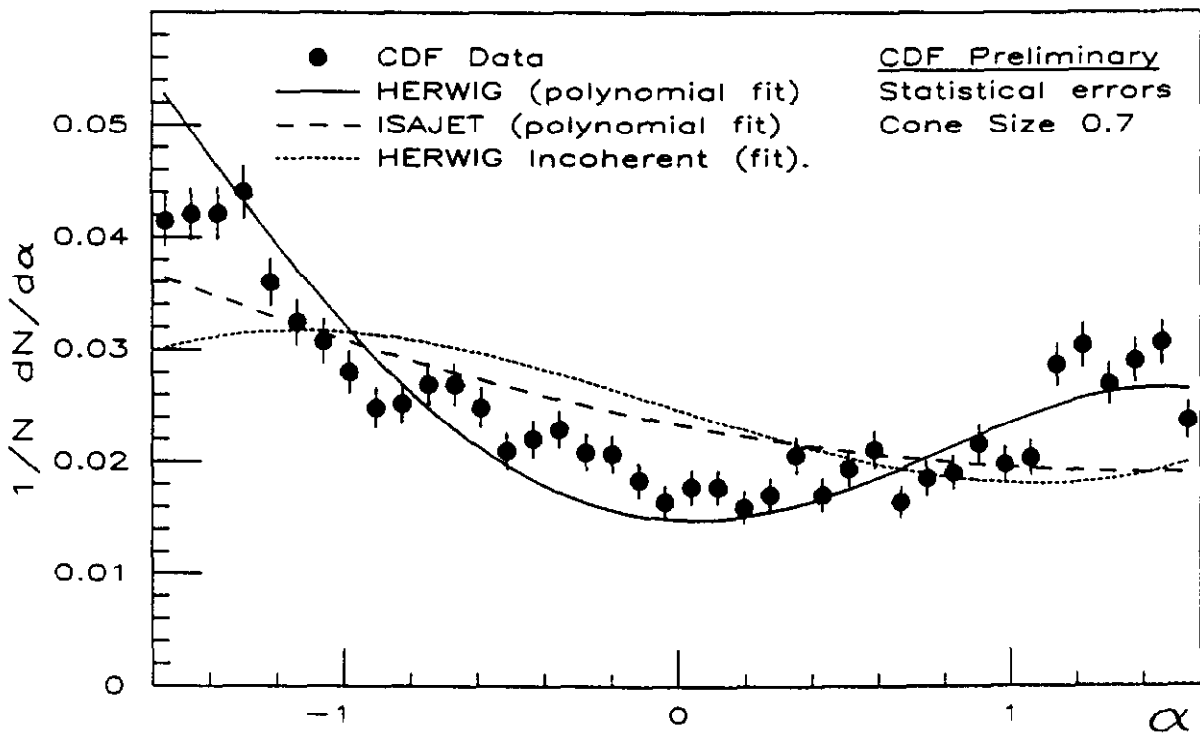


Figure 7: The α distribution of CDF data compared to the predictions of HERWIG and ISAJET. The signal for QCD interference is an increasingly positive slope as $\alpha \rightarrow \pi/2$ (equivalent to an excess of events in the enhancement region of Fig. 6c.)

2. Testing QCD with Photons

Prompt photons are produced in the initial $\bar{p}p$ collision, in contrast to photons produced by decays of hadrons. We define a photon ¹⁵⁾ as one or two towers of energy in the electromagnetic calorimeter (CEM), with less than 11% hadronic energy and no charged track. Jet backgrounds were reduced by requiring the photon to be *isolated*: the extra transverse energy inside a cone of radius $R = \sqrt{(\Delta\eta)^2 + (\Delta\phi)^2} = 0.7$ around the photon is less than 2 GeV. The remaining background is dominated by isolated single π^0 and η mesons. Two background subtraction methods were used: the *profile method* uses a χ^2 test of the transverse profile of the photon measured in strip chambers (CES) embedded at shower maximum in the CEM, and the *conversion method* counts the number of conversion pairs in the central drift tubes (CDT). The profile methods efficiency, for photons and background, has been simulated with testbeam electrons and checked against electrons from W decay, photons from η decay, and π^0 s from ρ decay. The conversion methods efficiency is P_T independent; it has been measured from photons and π^0 s, and agrees with the amount of material in the detector. The two methods give the same cross section in their common region of P_T .

2.1. Isolated Single Photon Cross Section

The isolated photon cross section from CDF ¹⁵⁾ and UA2 ¹⁶⁾ is shown in Fig. 8a compared to QCD calculations ¹⁷⁾ at next to leading order (except photon *bremsstrahlung* is only included at leading order). The inner error bars are the statistical error and the outer error bars are the statistical and P_T dependent systematic uncertainty combined in quadrature. The P_T independent component of the systematic uncertainty is shown as the normalization uncertainty. The QCD prediction changes within 30% when the structure functions are varied among commonly used sets, and changes by 12% when the renormalization scale is halved or doubled. The measured cross section agrees qualitatively with QCD calculations but has a steeper slope at low P_T . Including *bremsstrahlung* at next-to-leading order in the calculation may improve the comparison ¹⁸⁾ and allow a measurement of the gluon distribution from these data.

2.2. Photon + Jet CMS Angular Distribution

Photon events contain jets; in the lowest order picture there is a single jet azimuthally opposite the photon. For this analysis we define the jet axis to be the momentum weighted vector sum of the axes of the three highest P_T CDF jets with $P_T > 10$ GeV and azimuthal separation from the photon $\Delta\phi_{\gamma j} > 120^\circ$. The three lab frame variables are the photon's P_T and pseudorapidity, η_γ , and the jet's pseudorapidity, η_{jet} . The jet's P_T is not used. The three CMS variables are

$$\eta^* = (\eta_\gamma - \eta_{jet})/2, \quad \eta_{boost} = (\eta_\gamma + \eta_{jet})/2, \quad P^* = P_T \cosh \eta^* \quad (2)$$

and the cosine of the CMS angle is $\cos \theta^* = \tanh \eta^*$. For $23 < P_T < 45$ GeV, we form two regions that have uniform acceptance in the CMS variables: Region 1 is ($0.0 < \eta^* < \pm 0.7$, $\mp 0.2 < \eta_{boost} < \pm 0.9$, $29 < P^* < 45$ GeV) and Region 2 is ($\pm 0.3 < \eta^* < \pm 1.1$, $\mp 1.2 < \eta_{boost} < \mp 1.2$, $38 < P^* < 47$ GeV). The two regions are normalized to each other using the overlap in $\cos \theta^*$. In Fig. 8b the photon+jet $\cos \theta^*$ distribution is compared to leading order and next-to-leading order calculations ¹⁹⁾; QCD predicts a fairly flat distribution resulting from subprocesses with s and t-channel quark exchange (spin 1/2). Also in Fig. 8b we

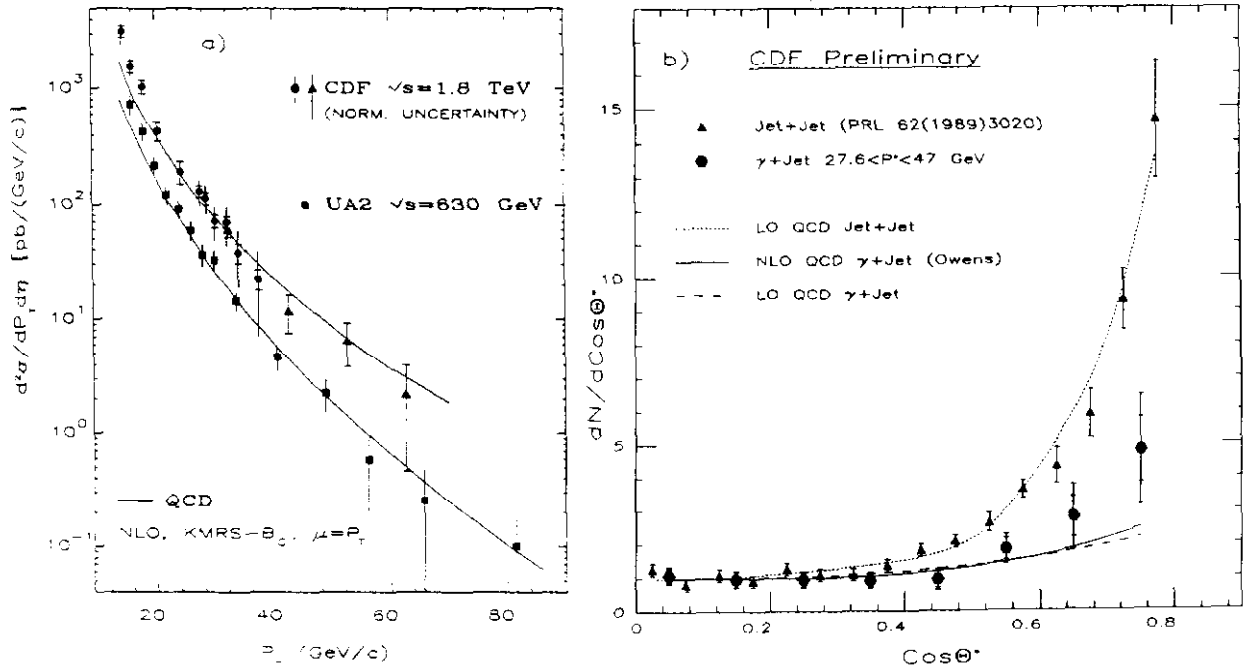


Figure 8: a) The isolated prompt photon cross section is compared to QCD. b) The CMS angular distribution for photon+jet and jet+jet events is compared to QCD.

show the $\cos\theta^*$ distribution for jet+jet events⁹⁾ compared to leading order calculations; QCD predicts a Rutherford-like scattering distribution resulting from subprocesses with t-channel gluon exchange (spin 1).

2.3. Isolated Double Photon Cross Section

In addition to probing the gluon distribution and testing QCD, production of two photons is an important background to $Higgs \rightarrow \gamma\gamma$ at the SSC. The three types of subprocesses which contribute to the cross section for promptly producing two photons (diphotons) are the *Born* diagram ($qq \rightarrow \gamma\gamma$), the *box* diagram ($gg \rightarrow \gamma\gamma$), and diagrams with photon *bremstrahlung*. CDF triggers on these events by requiring two clusters of electromagnetic energy, each with at least 10 GeV P_T . Cuts similar to those for single photons are employed, however, the isolation cut on each photon requires that the sum of the neighboring towers is less than 10% of the photon energy. For photons with $10 < P_T < 35$ GeV, there are 149 diphoton candidates (298 photons). The backgrounds from isolated $\gamma\pi^0$ and $\pi^0\pi^0$ events are subtracted using the *profile* method. Roughly one third of the sample are true di-photons (40% if we restrict ourselves to photons with $10 < P_T < 19$ GeV). In Fig. 9a we show the di-photon cross section as a function of the P_T of each photon; each event has two entries in the plot. The di-photon cross section is compared to NLO QCD and leading order QCD (both calculations include *bremstrahlung* at leading order), as well as the individual contributions of the Born diagram and Box diagram.²⁰⁾ The CDF diphoton data is significantly above the QCD prediction, similar to the single photons at low P_T , and the UA2 measurement of di-photons in their lowest P_T bin.²¹⁾ Including *bremstrahlung* at next-to-leading order in the calculation may improve the comparison.¹⁸⁾

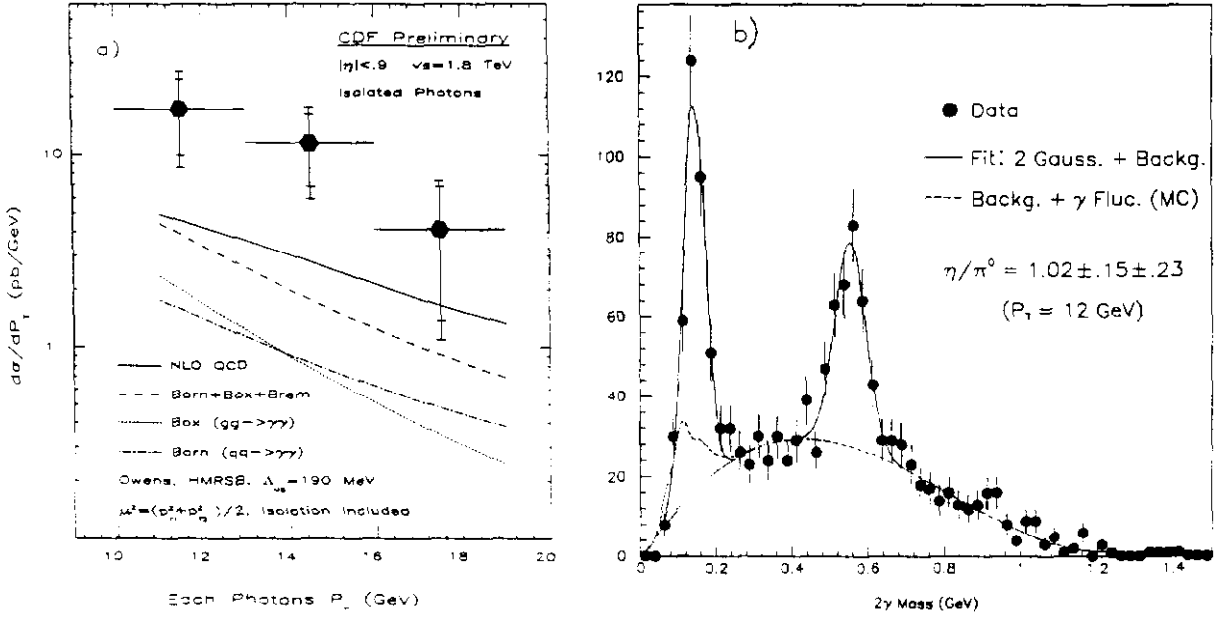


Figure 9: a) The isolated double prompt photon cross section compared to QCD predictions. ²⁰⁾ b) The invariant mass of two non-prompt photons (NOT the di-photon mass) shows peaks from isolated π^0 and η mesons.

2.4. Isolated Meson Production Ratio η/π^0

Isolated η and π^0 mesons are the primary background to prompt photons, so their relative production rates is of some interest. Also, the isolation requirement, described in section 2, may enhance the fraction of promptly produced mesons ²²⁾ relative to mesons from jet fragmentation. We use small CES clusters (25 mrad), to separate the closely spaced photons from π^0 s as well as η s, and require the two highest energy CES clusters to be in the adjoining CEM towers of a single isolated EM cluster. Multi- π^0 backgrounds are reduced by requiring the energy sum of extra CES clusters in the EM cluster be less than 30% of the sum of the highest two. Misidentification of single photon showers as a π^0 at the tower boundary is reduced by requiring the two tower's energy asymmetry ($|E_1 - E_2|/(E_1 + E_2)$) to be less than 0.8. In Fig. 2c the two photon mass distribution shows the π^0 and η peaks; this is fit with two gaussians and a polynomial-like background ($\chi^2/DOF = .95$). Also shown is the estimated amount of single photons misidentified as π^0 s. Subtracting the backgrounds, and using the relative acceptances of π^0 s and η s from a full trigger and detector simulation, we obtain a production ratio $\eta/\pi^0 = 1.02 \pm .15(stat) \pm .23(sys)$. The CDF measurement, for isolated mesons with mean P_T of 12 GeV, is within 1.3σ of the UA2 measurement ²³⁾ of $0.60 \pm .04 \pm .15$ for non-isolated mesons with mean P_T of 4.5 GeV.

3. Conclusions

Most measurements of jets at CDF are quantitatively consistent with the predictions of current QCD calculations. The inclusive jet cross section agrees with QCD and has been used to exclude HMRSE structure functions and set a limit on quark compositeness ($\Lambda_C > 1.4$ TeV at 95% CL). Two jet angular distributions are also in agreement with QCD and have been used to set a limit on quark compositeness ($\Lambda_C > 1.0$ TeV at 95% CL). However, the ratio of scaled cross sections at $\sqrt{s} = 546$ and 1800 GeV is not in good agreement with either scaling or QCD. Finally, soft third jet production shows an

effect compatible with QCD interference (color coherence). The next CDF running period, beginning in 1992, should provide 5 times more statistics at the highest jet P_T .

Most measurements of isolated prompt photons at CDF are only in qualitative agreement with current QCD calculations (these calculations may be underestimating the *bremsstrahlung* contribution¹⁸⁾). The single prompt photon cross section has a steeper slope at low P_T than predicted by QCD. Prompt photon plus jet angular distributions are in rough agreement with QCD at higher P_T , implying an angular distribution dominated by spin 1/2 quark exchange in the s and t-channel. Double prompt photon production is significantly greater than predicted by NLO QCD, and hence will contribute a much larger background to the process $\text{Higgs} \rightarrow \gamma\gamma$ than previously expected. Our measurement of the *isolated* production ratio of η and π^0 mesons at 12 GeV is $(\bar{p}p \rightarrow \eta + X)/(\bar{p}p \rightarrow \pi^0 + X) = 1.02 \pm .15(\text{stat}) \pm .23(\text{sys})$, within 1.3σ of the UA2 measurement for non-isolated mesons at lower P_T . For the 1992 run we have a new photon conversion detector just outside the solenoidal coil ($1 X_0$), which should allow an order of magnitude increase in statistics and decreased systematic uncertainties for prompt photon measurements over a wide range of P_T .

References

1. F. Abe *et al.* (CDF Collaboration), *Nucl. Instr. Meth.* **A271**(1988)387.
2. S. Ellis, Z. Kunszt, D. Soper, *Phys. Rev. Lett.* **64**(1990)2121.
3. R. Ellis and J. Sexton, *Nucl. Phys.* **B269**(1986)445.
4. F. Aversa *et al.*, *Phys. Lett.* **B210**(1988)225.
5. E. Eichten, K. Lane, M. Peskin, *Phys. Rev. Lett.* **50**(1983)811.
6. F. Abe, *et al.* (CDF Collaboration), *Phys. Rev. Lett.* **68**(1992)1104.
7. F. Abe, *et al.* (CDF Collaboration), *Phys. Rev. Lett.* **62**(1989)613.
8. P. Harriman, A. Martin, R. Roberts, W. Stirling *Phys. Rev.* **D42** (1990)798, *Phys. Lett.* **B243**(1990)421. J. Morfin and W. Tung, *Z. Phys.* **C52**(1991)13.
9. F. Abe, *et al.* (CDF Collaboration), *Phys. Rev. Lett.* **62**(1989)3020.
10. J. Appel, *et al.*, *Phys. Lett.* **B160**(1985)349.
11. R. K. Ellis, G. Marchesini and B. R. Webber, *Nucl. Phys.* **B286**(1987)643 and references therein.
12. S. Catani, M. Ciafaloni and G. Marchesini. *Nucl. Phys.* **B264**(1986)588.
13. F. E. Paige and S. D. Protopescu, BNL Report 37066.
14. G. Marchesini and B. R. Webber, *Nucl. Phys.* **B310**(1988)461.
15. F. Abe *et al.* (CDF Collaboration), *Phys. Rev. Lett.* **68**(1992)2734.
16. J. Alitti, *et al.* (UA2 Collaboration), CERN-PPE/91-68, 1991.
17. H. Baer, J. Ohnemus, and J. F. Owens *Phys. Lett.* **B234**(1990)127.
18. J. P. Guillet in these proceedings, and E. Pilon in last years proceedings of the XXVI Recontre de Moriond (1991).
19. We appropriately modified the computer program of reference 17.
20. J. F. Owens in these proceedings, also B. Bailey, J. F. Owens and J. Ohnemus, FSU-HEP-920320 (1992). These theory curves replace the curve in Fig. 2a on page 720 of the Proceedings of the Vancouver Meeting of Particles and Fields, Aug 18-22, 1991, and also in FERMILAB-CONF-91-236-E. The old curves in that figure were incorrectly labelled PYTHIA (we apologize to the authors of PYTHIA).
21. C. Talamonti (UA2 Collaboration) in these proceedings.
22. M. Benayoun, *et al.*, *Nucl. Phys.* **B282**(1987)653.
23. M. Banner, *et al.* (UA2 Collaboration), *Z. Phys.* **C27** (1985)329.